Research Square

Preprints are preliminary reports that have not undergone peer review.
They should not be considered conclusive, used to inform clinical practice,
or referenced by the media as validated information.

Deep Learning Reconstruction for 40-keV Virtual Monoenergetic CT of Colon Cancer: Evaluation of Image Quality and Edge Sharpness

Yuhan Bao
the Affiliated Hospital of Xuzhou Medical University
Juan Long
the Affiliated Hospital of Xuzhou Medical University
Zhen Wang
the Affiliated Hospital of Xuzhou Medical University
Xiaohan Liu
the Affiliated Hospital of Xuzhou Medical University
Chen Wu
the Affiliated Hospital of Xuzhou Medical University
Haini Zhang
the Affiliated Hospital of Xuzhou Medical University
Mingyue Zhou
the Affiliated Hospital of Xuzhou Medical University
Chong Meng
the Affiliated Hospital of Xuzhou Medical University
Zhongxiao Liu
the Affiliated Hospital of Xuzhou Medical University
Aiyun Sun
GE HealthCare China
Kai Xu
the Affiliated Hospital of Xuzhou Medical University
Yankai Meng
mengyankai@126.com

the Affiliated Hospital of Xuzhou Medical University

Research Article

Keywords: Colon Neoplasms, Computed Tomography, Dual-Energy, Deep Learning, Image Reconstruction, Virtual Monoenergetic Imaging, Contrast-to-Noise Ratio, Image Quality

Posted Date: January 21st, 2026

DOI: https://doi.org/10.21203/rs.3.rs-8621121/v1

License: This work is licensed under a Creative Commons Attribution 4.0 International License.
Read Full License

Additional Declarations: No competing interests reported.

Version of Record: A version of this preprint was published at Abdominal Radiology on April 6th, 2026. See the published version at https://doi.org/10.1007/s00261-026-05494-1.

Deep Learning Reconstruction for 40-keV Virtual Monoenergetic CT of Colon Cancer: Evaluation of Image Quality and Edge Sharpness

Manuscript drafting or manuscript revision for important intellectual content: All authors

Approval of final version of submitted manuscript: All authors.

Disclosure of Conflicts of Interest:

The authors of this manuscript declare no relationships with any companies, whose products or services may be related to the subject matter of the article.

Grant support:

This study was funded by the Special Fund for Overseas Training of Employees of the Affiliated Hospital of Xuzhou Medical University.

Word count: 3642 words (5 Figures, 5 Tables, and 1 Supplementary Table)

Running title: Deep Learning Reconstruction for 40-keV CT of Colon Cancer

Abbreviation index

ASIR-V: Adaptive statistical iterative reconstruction-V

CNR: Contrast-to-noise ratio

$CTDI_{vol}$: Volume CT dose index

DECT: Dual-energy CT

DLIR: Deep learning image reconstruction

DLIR-H: High-strength DLIR

DLIR-M: Medium-strength DLIR

ERD: Edge rise distance

ERS: Edge rise slope

SNR: Signal-to-noise ratio

VMI: Virtual monoenergetic imaging

Abstract

Background:

Virtual monoenergetic imaging (VMI) at 40 keV improves iodine attenuation in colon cancer CT but is constrained by severe image noise. Deep learning image reconstruction (DLIR) may address this limitation, but its effect on anatomical edge preservation across multiple targets requires investigation.

Purpose:

To evaluate the impact of DLIR on objective and subjective image quality of 40-keV VMIs in colon adenocarcinoma, with emphasis on the trade-off between noise reduction and edge definition.

Materials and Methods:

In this retrospective study (May 2024–February 2025), 60 patients (mean age, 62.8 years ± 15.1; 34 men) with confirmed colon adenocarcinoma underwent dual-energy CT using a low-iodine protocol (1.0 mL/kg). Portal venous phase data were reconstructed at 40 keV using adaptive statistical iterative reconstruction-V (ASIR-V) 50%, medium-strength DLIR (DLIR-M), and high-strength DLIR (DLIR-H). Contrast-to-noise ratio (CNR), signal-to-noise ratio (SNR), and edge rise slope (ERS) were measured for tumors, feeding arteries, and regional lymph nodes. Two radiologists scored overall quality and boundary definition (5-point Likert scale). Data were compared using the Friedman test and post-hoc Bonferroni correction.

Results:

DLIR-H yielded the lowest image noise and highest CNR and SNR across all anatomical targets compared with DLIR-M and ASIR-V 50% (all $P < .001$). For colon tumors, the CNR of DLIR-H (5.4±2.2) was 82% higher than that of ASIR-V 50% (3.0±1.1, $P < .001$). Although ASIR-V 50% maintained a higher ERS than DLIR-H (108.0±15.2 vs 101.4±14.1 HU/mm, $P < .001$), DLIR-H received the highest subjective scores for overall image quality and lesion boundary definition (median, 5.0 [IQR: 4.0–5.0] vs 3.0 [IQR: 2.0–3.0]; $P < .001$).

Conclusion:

In 40-keV virtual monoenergetic CT of colon cancer, DLIR-H significantly improves image quality for tumors, vessels, and lymph nodes. While a minor objective edge-smoothing effect exists, DLIR-H provides an optimal balance between robust noise suppression and anatomical clarity, facilitating low-iodine spectral protocols.

Keywords: Colon Neoplasms; Computed Tomography, Dual-Energy; Deep Learning; Image Reconstruction; Virtual Monoenergetic Imaging; Contrast-to-Noise Ratio; Image Quality.

Clinical Impact:

1. High-strength deep learning image reconstruction (DLIR-H) facilitates the routine clinical adoption of 40-keV virtual monoenergetic imaging in colon cancer by overcoming the severe noise limitations of iterative reconstruction.
2. By providing superior visualization of the primary tumor-to-fat interface, vascular anatomy, and regional lymph nodes, DLIR-H supports more confident preoperative T-staging and surgical planning for root lymphadenectomy.
3. The synergy between DLIR and low-keV imaging enables a "low-iodine dose" protocol (1.0 mL/kg), offering a safer diagnostic pathway for patients with renal impairment or those requiring repeated CT surveillance without compromising image quality.

Highlights:

1. At 40-keV virtual monoenergetic CT, high-strength deep learning reconstruction (DLIR-H) reduces image noise by 82% and significantly improves the contrast-to-noise ratio for colon tumors, regional lymph nodes, and mesenteric feeding arteries compared with ASIR-V.
2. Although DLIR-H results in a minor objective reduction in the edge rise slope, it yields superior qualitative scores for lesion boundary definition and overall image quality compared with iterative reconstruction.
3. The synergy between DLIR-H and 40-keV virtual monoenergetic imaging facilitates high-fidelity preoperative assessment of colon cancer using a low-iodine contrast protocol (1.0 mL/kg).

Introduction

Colorectal cancer (CRC) remains the third most prevalent malignancy and a leading cause of cancer-related mortality worldwide, accounting for over 1.9 million new cases and nearly 930,000 deaths annually[1, 2]. Accurate preoperative staging and the identification of high-risk morphological features are essential for determining individualized therapeutic strategies, such as selecting candidates for neoadjuvant therapy or determining the extent of surgical resection[3, 4]. Although multidetector CT remains the clinical mainstay for preoperative staging, its sensitivity for identifying subtle morphological indicators—such as early serosal invasion (pT3) or small metastatic lymph nodes—is frequently hampered by insufficient contrast-to-noise ratios (CNR) in conventional polychromatic imaging[5-7].

Spectral dual-energy CT (DECT) provides a robust solution to these constraints through virtual monoenergetic imaging (VMI). Specifically, 40-keV VMIs leverage the photoelectric effect by approaching the K-edge of iodine (33.2 keV), which substantially boosts the attenuation of iodinated structures. This physical advantage translates into markedly improved conspicuity of hypervascular tumors, enhanced definition of the mesenteric feeding arteries, and more sensitive detection of regional lymph nodes[8, 9]. Nevertheless, the clinical implementation of 40-keV VMI is frequently constrained by a prohibitive increase in image noise and photon starvation. These phenomena can compromise textural fidelity and mask subtle anatomical landmarks, such as the tumor-to-fat interface, which are essential for precise colorectal cancer staging[10, 11].

Standard-of-care hybrid iterative reconstruction (IR), such as adaptive statistical iterative reconstruction-V (ASIR-V), is intrinsically limited by its linear-blending architecture. At higher strength settings, these algorithms often introduce unnatural image textures—frequently characterized as a 'waxy' or 'blotchy' appearance—and can lead to a degradation of spatial resolution and anatomical fidelity[12, 13]. More recently, deep learning image reconstruction (DLIR) has emerged as a transformative approach,

employing deep convolutional neural networks to intelligently distinguish between anatomical signal and image noise[14]. While preliminary evidence in liver and pancreatic imaging suggests that DLIR can substantially suppress noise while preserving textural integrity[15, 16], its impact on the comprehensive, multi-target assessment of colon cancer—encompassing the primary tumor, vascular anatomy, and regional lymph nodes—remains largely underexplored.

Crucially, in oncologic imaging, a reduction in image noise does not inherently translate to improved diagnostic performance. While conventional metrics such as CNR and signal-to-noise ratio (SNR) quantify signal conspicuity, they fail to account for spatial resolution and structural fidelity—critical factors for delineating the tumor-to-fat interface and vascular margins. To date, it remains unclear whether high-strength DLIR, despite achieving profound noise suppression at 40 keV, preserves the sharpness required for precise staging. Quantitative sharpness metrics, specifically edge rise distance (ERD) and edge rise slope (ERS), are therefore essential to objectively characterize the potential trade-off between denoising and edge smoothing in this high-contrast spectral environment[17-19].

Therefore, the purpose of our study was to compare the objective and subjective image quality of 40-keV VMIs reconstructed with DLIR versus ASIR-V in patients with colon adenocarcinoma. We aimed to evaluate the reconstruction performance across three critical clinical targets—the primary tumor, feeding arteries, and regional lymph nodes—while specifically investigating the balance between noise suppression and edge preservation using ERD and ERS.

Materials and Methods

Study Population

This retrospective study was approved by our institutional review board (Approval No. XYFY2023-KL229), and written informed consent was obtained from all patients. The study was conducted in accordance with the Declaration of Helsinki.

Between May 2024 and February 2025, we consecutively identified patients with suspected colon cancer who underwent preoperative dual-energy CT (DECT) at our institution. The inclusion criteria were as follows: (a) age ≥ 18 years; (b) pathologically confirmed colon adenocarcinoma; and (c) no prior anti-tumor treatment before the DECT scan. Patients were excluded for the following reasons: (a) known allergies to iodinated contrast agents (n = 2); (b) hyperthyroidism (n = 2); (c) severe cardiovascular, hepatic, or renal dysfunction (n = 1); or (d) significant motion artifacts or inability to cooperate (n = 3). The patient selection process is summarized in **Figure 1**.

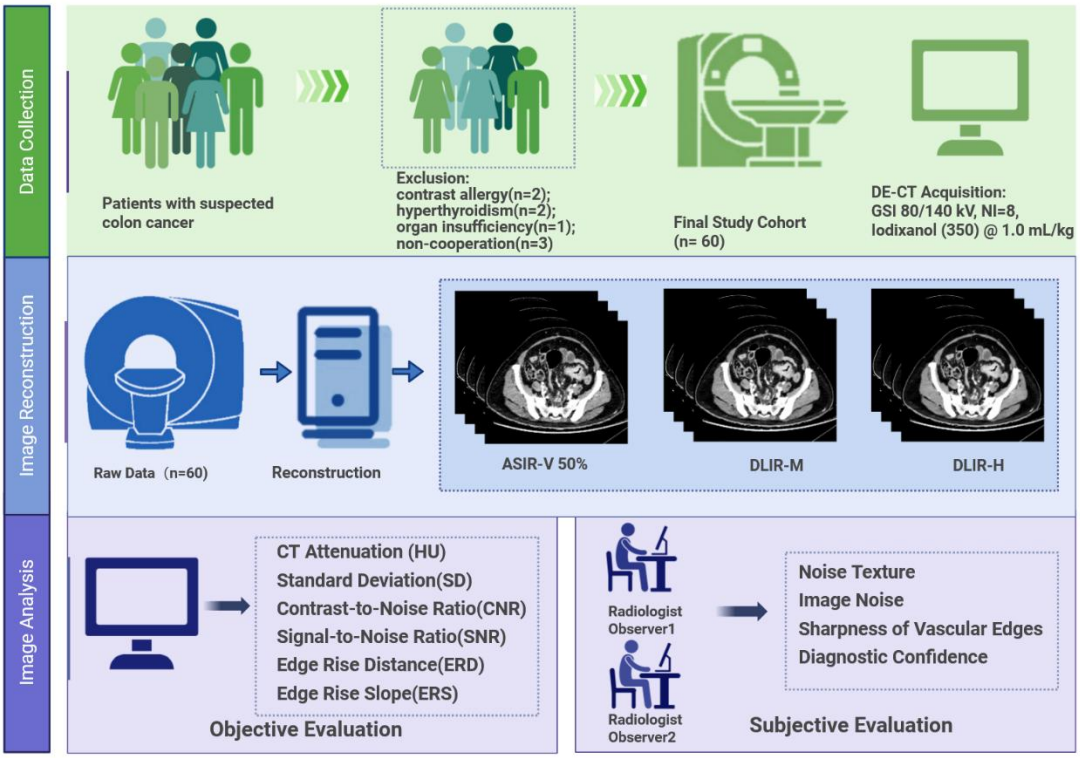


Figure 1 Flowchart of the retrospective study.

CT Acquisition and Contrast Protocol

All patients underwent dual-energy CT (DECT) using a 256-slice scanner (Revolution CT; GE Healthcare, Waukesha, Wis) in Gemstone Spectral Imaging (GSI) mode. Scans were performed in the supine position from the diaphragmatic dome to the symphysis pubis.

Scanning parameters were as follows: instantaneous tube voltage switching between 80 and 140 kVp (switching time, 0.5 msec); automatic tube current (range, 300–600 mA); noise index (NI), 11.0; detector collimation, 128×0.625 mm; pitch, 0.984; and rotation time, 0.5 sec.

The contrast protocol included a nonionic iodinated contrast medium (iohexol, 300 mgI/mL; GE Healthcare, Shanghai, China) administered intravenously via an antecubital vein at a dose of 1.0 mL/kg (injection rate, 2.2 mL/sec). This was followed by a 30-mL saline flush. Bolus tracking was performed with a region of interest (ROI) placed in the abdominal aorta. The scan was triggered 5 seconds after the attenuation reached a threshold of 150 Hounsfield units (HU) for the arterial phase, followed by a 38-second delay for the portal venous phase.

Image Reconstruction

Spectral data from the portal venous phase were used to generate virtual monoenergetic images (VMI) at 40 keV. Three different reconstruction algorithms were applied for comparison:

ASIR-V 50%: Adaptive statistical iterative reconstruction-V (GE Healthcare) at a 50% blending level, which served as the clinical reference standard.

DLIR-M: Deep learning image reconstruction (TrueFidelity; GE Healthcare) at the medium-strength setting.

DLIR-H: Deep learning image reconstruction at the high-strength setting[14].

All images were reconstructed with a slice thickness of 1.25 mm and a reconstruction interval of 0.625 mm.

Objective Image Quality Analysis

Quantitative image quality metrics were evaluated by a radiologist (C.W., with 10 years of experience in abdominal imaging) on a dedicated workstation (Advantage Workstation 4.7; GE Healthcare). For each patient, mean attenuation (in Hounsfield

units [HU]) and standard deviation (SD) were measured using circular regions of interest (ROIs) across the three reconstruction sets. To ensure consistency, all ROIs were first delineated on the ASIR-V50% images and then propagated to the DLIR-M and DLIR-H datasets using the copy-and-paste function.

Measurements were performed for the following anatomical targets:

I. Colon tumor: ROIs were placed at the level of the maximal transverse diameter of the tumor. The ROIs were positioned within the homogeneous solid component, strictly avoiding areas of cystic change, necrosis, hemorrhage, gas, or calcification.

II. Feeding artery: The ileocolic artery was identified as the primary feeding vessel. Measurements were obtained at a level 2 cm inferior to the origin of the ileocolic artery. ROIs were centered within the vessel lumen, ensuring that any mural calcifications were excluded.

III. Regional lymph node: The largest peritumoral lymph node was identified for each patient. ROIs were placed within the center of the node at its maximal dimension.

Background Noise and Calculations

Image noise was defined as the SD of an ROI placed in the muscle at the same anatomical level as the primary tumor (either the psoas major or the gluteus maximus muscle, depending on the tumor location).

The contrast-to-noise ratio (CNR) and signal-to-noise ratio (SNR) were calculated using the following formulas:

$$CNR = \frac{Attenuationtumor - Attenuationmuscle}{SDmuscle}$$

$$SNR = \frac{Attenuationtumor}{SDmuscle}$$

Image Sharpness and Edge Metrics

Image sharpness was objectively assessed using the edge rise distance (ERD) and edge rise slope (ERS). A line-density profile was drawn perpendicular to the interface between the tumor and the adjacent pericolonic fat using ImageJ software (version 1.53; National Institutes of Health, Bethesda, Md). The ERD (in millimeters) was defined as the spatial distance between the 10% and 90% positions of the maximum attenuation rise along the profile. The ERS (in HU/mm) was calculated as follows:

$$ERS = \frac{HU90\% - HU10\%}{ERD}$$

Subjective Image Quality Evaluation

Two radiologists (Y.K.M. and K.X., with 20 and 30 years of experience in gastrointestinal imaging, respectively), who were blinded to the clinical data and the reconstruction algorithms, independently evaluated the 40-keV VMI datasets in a randomized order. To minimize recall bias, a 2-week washout period was implemented between the evaluation of different reconstruction sets for the same patient.

Qualitative image quality was assessed using a 5-point Likert scale (1 = poor, 5 = excellent; **Supplementary Table E1**). The assessment encompassed four distinct categories: (a) overall image quality, (b) image noise, (c) lesion contrast, and (d) lesion boundary definition. A score of 3 or higher was pre-defined as the threshold for meeting clinical diagnostic requirements.

Images were displayed on a dedicated clinical PACS workstation (Advantage Workstation 4.7; GE Healthcare) under standardized ambient lighting conditions. Readers were permitted to adjust the window width and level settings to achieve optimal visualization of the tumor and its surrounding structures. In the event of a score discrepancy, a final consensus score was reached through joint discussion between the two readers.

Supplementary Table E1 5-point Likert scale

Score	Overall Quality	Image Noise	Lesion Contrast	Boundary Definition
1 (Poor)	Non-diagnostic	Severe; assessment impossible	Very poor; unidentifiable	Unidentifiable; lost demarcation
2 (Fair)	Suboptimal; low confidence	Noticeable; interferes with evaluation	Poor; hampers evaluation	Blurry; poorly defined margins
3 (Moderate)	Acceptable; meets basic needs	Moderate; mildly affects assessment	Average; subtle effect	Moderate; some unclear segments
4 (Good)	Good; sufficient for diagnosis	Minimal; no interference	Good; confident evaluation	Mostly clear; well-defined margins
5 (Excellent)	Excellent; optimal texture	None; optimal appearance	Optimal; excellent conspicuity	Distinct; sharp demarcation

Note.—The 5-point Likert scale was used independently by two senior radiologists to evaluate the 40-keV virtual monoenergetic images across all reconstruction groups. A score of 3 or higher was considered to meet the requirements for clinical diagnosis.

Radiation Dose Parameters

Radiation dose parameters, including the volume CT dose index ($CTDI_{vol}$) and dose-length product (DLP), were obtained from the electronic dose report automatically generated by the CT scanner for each examination. The effective dose (ED) was estimated by multiplying the DLP by a normalized conversion factor (k) for the abdomen and pelvis (k = 0.015 $mSv \cdot mGy^{-1} \cdot cm^{-1}$), consistent with the International Commission on Radiological Protection (ICRP) Publication 10[3].

Statistical Analysis

Statistical analyses were performed using SPSS software (version 26.0; IBM, Armonk, NY). Data were tested for normality using the Shapiro-Wilk test. Continuous variables were expressed as means ± standard deviations (SD) for normally distributed data or as medians with interquartile ranges (IQR) for non-normally distributed data.

Differences in objective image quality metrics and radiation doses among the three

reconstruction groups (ASIR-V 50%, DLIR-M, and DLIR-H) were compared using repeated-measures one-way analysis of variance (ANOVA) or the Friedman test, as appropriate. When significant differences were identified, post-hoc pairwise comparisons were conducted with Bonferroni correction to adjust for multiple comparisons. Inter-reader agreement for the qualitative subjective scores was assessed using the weighted kappa (κ) statistic, with agreement levels interpreted as follows: 0.00–0.20, poor; 0.21–0.40, fair; 0.41–0.60, moderate; 0.61–0.80, good; and 0.81–1.00, excellent agreement. A two-tailed *P* value less than .05 ($P < .05$) was considered to indicate a statistically significant difference.

Results

Study Population and Radiation Dose

A total of 60 patients with pathologically confirmed colon adenocarcinoma were identified and included (34 men, 26 women; mean age, 62.8±15.1 years). The mean body mass index (BMI) was 23.1±3.4 kg/m^2. Fifty-seven percent of patients (n = 34) were within the normal weight range (BMI, 18.5–23.9 kg/m^2).

The mean iodine contrast agent volume was 65.0±14.4 mL with an injection rate of 2.2±0.5 mL/sec. Radiation dose metrics were as follows: mean $CTDI_{vol}$, 10.9±1.9 mGy; mean DLP, 594.2±136.4 mGy·cm; and estimated mean ED, 8.9±2.1 mSv. Patient demographics and dose parameters are summarized in **Table 1**.

Table 1. Patient Demographics, Contrast Media Parameters, and Radiation Dose Metrics (*N* = 60)

Characteristic	Value
Demographics	
Age (y) *	62.8±15.1

Sex	
Men	34(57)
Women	26(43)
BMI (kg/m^2) †	
Underweight (< 18.5)	2(3)
Normal weight (18.5–23.9)	34(57)
Overweight or obese (≥ 24.0)	24(40)
Contrast Media Parameters	
Iodine contrast volume (mL) *	65.0±14.4
Injection rate (mL/sec) *	2.2±0.5
Radiation Dose	
$CTDI_{vol}$ (mGy) *	10.9±1.9
DLP (mGy.cm) *	594.2±136.4
Effective dose (mSv) *	8.9±2.1

Note.—Unless otherwise specified, data are numbers of patients, with percentages in parentheses.

*Data are means ± standard deviations.

†BMI categories are based on regional health standards used at our institution.

BMI = body mass index, CTDIvol = volume CT dose index, DLP = dose-length product, ED = effective dose.

Objective Image Quality Evaluation

CT Attenuation and Image Noise

At the 40-keV level, there were no significant differences in CT attenuation for the colon tumor, feeding artery, or regional lymph nodes among the three reconstruction

algorithms (all $P > .90$; **Table 2**). However, image noise was highest in the ASIR-V50% group and significantly decreased with DLIR, reaching the lowest levels in the DLIR-H group ($P < .001$). For colon tumors, image noise was reduced by 38% with DLIR-H (24.7 HU±5.1) compared with ASIR-V50% (39.7 HU±7.4).

SNR and CNR

Both CNR and SNR showed a progressive increase from ASIR-V50% to DLIR-M, reaching maximum values in the DLIR-H group ($P<.001$; **Table 2**, **Figure 2**). For colon tumors, DLIR-H yielded a CNR of 5.4±2.2 and an SNR of 11.3±2.5, representing significant improvements over the ASIR-V50% and DLIR-M reconstructions (all $P < .001$). Similar significant improvements in CNR and SNR were observed for the feeding artery and regional lymph nodes in the DLIR-H group.

Table 2. Objective Image Quality Parameters for Colon Tumor, Feeding Artery, and Lymph Nodes at 40 keV

Variable	ASIR-V 50%	DLIR-M	DLIR-H	*P*-Value
Colon Tumor				
Attenuation (HU)	200.1±33.5	199.3±33.1	198.5±32.8	0.97
Image noise (HU)	39.7±7.4	32.7±6.4	24.7±5.1	<.001
SNR	6.2±1.3	8.0±1.7	11.3±2.5	<.001
CNR	3.0±1.1	3.8±1.5	5.4±2.2	<.001
Feeding Artery				
Attenuation (HU)	367.9±54.7	370.6±54.4	368.8±54.0	0.96
Image noise (HU)	29.6±7.4	28.4±7.4	24.3±7.0	<.001
SNR	11.3±2.0	14.7±2.6	20.8±3.9	<.001

CNR	3.0±1.1	3.8±1.5	5.4±2.2	<.001
Regional Lymph Node				
Attenuation (HU)	213.7±45.9	217.4±48.1	215.4±48.9	0.91
Image noise (HU)	27.6±7.7	26.8±7.7	22.3±6.6	<.001
SNR	6.6±1.4	8.6±1.9	12.1±2.8	<.001
CNR	3.3±1.5	4.5±1.4	6.2±2.8	<.001

Note.—Data are means ± standard deviations.

ASIR-V = adaptive statistical iterative reconstruction-V, CNR = contrast-to-noise ratio, DLIR-H = high-strength deep learning image reconstruction, DLIR-M = medium-strength deep learning image reconstruction, HU = Hounsfield unit, SNR = signal-to-noise ratio.

Table 3. Pairwise Comparisons of Objective Image Quality Parameters among the Three Reconstruction Algorithms

Variable	ASIR-V 50% vs DLIR-M	ASIR-V 50% vs DLIR-H	DLIR-M vs DLIR-H
Colon Tumor			
Attenuation (HU)	.901	.794	.888
Image noise (HU)	<.001	<.001	.002
SNR	<.001	<.001	<.001
CNR	.007	<.001	<.001
Feeding Artery			
Attenuation (HU)	.786	.921	.862
Image noise (HU)	.382	<.001	.002
SNR	<.001	<.001	<.001

CNR	<.001	<.001	<.001
Regional Lymph Node			
Attenuation (HU)	.669	.845	.817
Image noise (HU)	.544	<.001	.001
SNR	<.001	<.001	<.001
CNR	<.001	.004	<.001

Note.—Data are *P* values, calculated using the Bonferroni-Dunn post-hoc test (or specified test from your methods). *P*<.05 was considered to indicate a statistically significant difference.

ASIR-V = adaptive statistical iterative reconstruction-V, CNR = contrast-to-noise ratio, DLIR-H = high-strength deep learning image reconstruction, DLIR-M = medium-strength deep learning image reconstruction, HU = Hounsfield unit, SNR = signal-to-noise ratio.

Image Sharpness and Noise Texture

Quantitative image sharpness metrics for the colon tumor are summarized in **Table 4**. There were no significant differences in the edge rise distance (ERD) among the three reconstruction groups (overall $P = .752$). However, the ERS demonstrated significant variations (overall $P < .001$).

Post-hoc pairwise comparisons revealed that ERS was significantly higher in the ASIR-V50% group (108.0 HU/mm [IQR, 88.7–129.2]) compared with the DLIR-H group (101.4 HU/mm [IQR, 85.4–115.2]; $P < .001$), suggesting a minor degree of objective edge smoothing associated with high-strength DLIR. No significant difference in ERS was observed between the ASIR-V50% and DLIR-M groups (P=.986), while DLIR-M maintained a significantly higher ERS than DLIR-H ($P = .008$).

Table 4. Objective Image Sharpness Parameters for Colon Tumor at 40 keV

Variable	ASIR-V 50%	DLIR-M	DLIR-H	Overall *P*	P_1	P_2	P_3
ERD (mm)	2.50 (1.99,2.90)	2.50 (2.17,2.87)	2.52 (2.05,2.87)	.752	.783	.621	.826
ERS (HU/mm)	108.0 (88.7,129.2)	106.1 (88.5,118.6)	101.4 (85.4,115.2)	<.001	0.986	<.001	.008

Note.—Data are medians, with interquartile ranges in parentheses. P_1 compares ASIR-V 50% vs DLIR-M, P_2 compares ASIR-V 50% vs DLIR-H, and P_3 compares DLIR-M vs DLIR-H. *P* values were calculated using the Kruskal-Wallis test followed by the Bonferroni-Dunn post-hoc test for multiple comparisons. $P < .05$ was considered to indicate a statistically significant difference.

ASIR-V = adaptive statistical iterative reconstruction-V, DLIR-H = high-strength deep learning image reconstruction, DLIR-M = medium-strength deep learning image reconstruction, ERD = edge rise distance, ERS = edge rise slope, HU = Hounsfield unit.

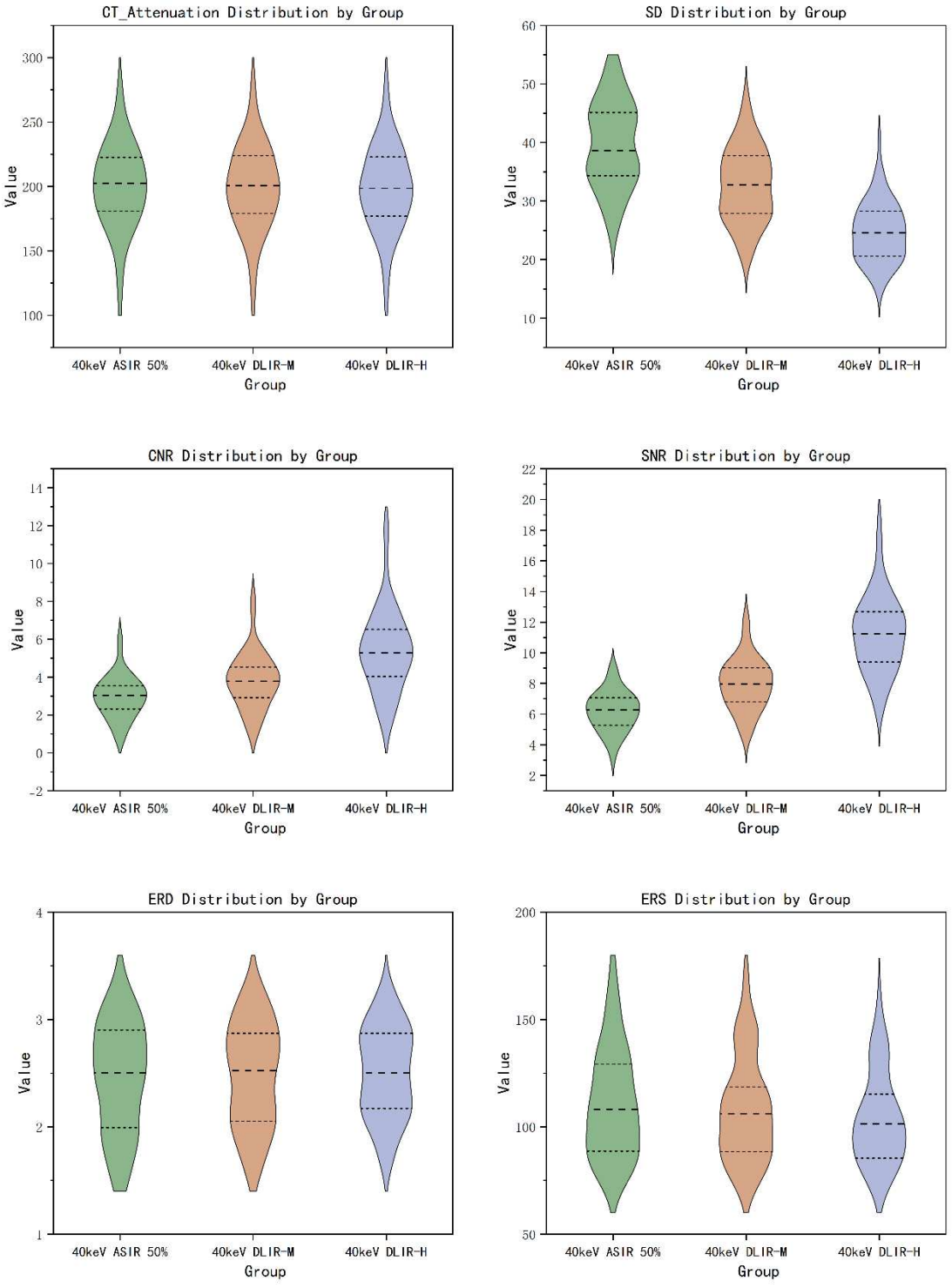


Figure 2: Quantitative objective image quality parameters across different reconstruction algorithms at 40-keV virtual monoenergetic imaging.

Violin plots illustrate the distribution and density of **(a)** CT attenuation, **(b)** image noise (standard deviation), **(c)** contrast-to-noise ratio (CNR), **(d)** signal-to-noise ratio (SNR), **(e)** edge rise distance (ERD), and **(f)** edge rise slope (ERS) for the ASIR-V 50%,

DLIR-M, and DLIR-H groups in patients with colon cancer. Within each violin plot, the solid horizontal lines represent the median values, and the dashed lines indicate the interquartile ranges (25th and 75th percentiles). Note the progressive reduction in image noise and substantial increase in CNR and SNR as the DLIR strength increases from medium (DLIR-M) to high (DLIR-H), while CT attenuation remains consistent across all groups.

ASIR-V = adaptive statistical iterative reconstruction-V, DLIR-H = high-strength deep learning image reconstruction, DLIR-M = medium-strength deep learning image reconstruction, HU = Hounsfield unit.

Subjective Image Quality Evaluation

Inter-reader Agreement

Inter-reader agreement was excellent across all subjective categories. The weighted κ values were .86 for overall quality, .85 for image noise, .91for lesion contrast, and .93 for lesion boundary (all $P < .001$). Detailed agreement metrics and scores are summarized in **Table 5**.

Subjective Scores

Significant differences were identified among the three reconstruction groups for all qualitative metrics (all $P < .001$; **Table 5**). DLIR-H consistently received the highest median scores (median, 5.0; IQR: 4.0–5.0) for overall image quality, noise reduction, and lesion visualization. In contrast, the ASIR-V50% group yielded the lowest ratings (median, 3.0; IQR: 2.0–3.0), indicating that while it met the baseline requirements for clinical diagnosis, it provided significantly less diagnostic confidence than the DLIR algorithms (**Figure 3**). Pairwise comparisons demonstrated that DLIR-H significantly outperformed both ASIR-V50% and DLIR-M in all categories (all $P < .001$).

Table 5. Qualitative Subjective Image Quality Assessment and Inter-reader

Agreement at 40 keV

Category	ASIR-V 50%	DLIR-M	DLIR-H	Kappa Value	Overall *P*	P_1	P_2	P_3
Overall quality	3.0(2.0,3.0)	3.0(3.0,4.0)	5.0(4.0,5.0)	.86	<.001	<.001	<.001	<.001
Image noise	3.0(3.0,3.0)	4.0(3.0,4.0)	5.0(4.0,5.0)	.85	<.001	<.001	<.001	<.001
Lesion contrast	3.0(2.0,3.0)	3.0(3.0,4.0)	4.0(4.0,5.0)	.91	<.001	<.001	<.001	<.001
Lesion boundary	3.0(3.0,3.0)	3.0(3.0,4.0)	4.0(4.0,5.0)	.93	<.001	<.001	<.001	<.001

Note.—Except for Kappa and *P* values, data are medians, with interquartile ranges in parentheses. Image quality was scored using a 5-point Likert scale (1 = poor, 5 = excellent). Inter-reader agreement was assessed using the weighted kappa (κ) statistic ($\kappa > 0.80$ indicates excellent agreement). P_1 compares ASIR-V 50% vs DLIR-M, P_2 compares ASIR-V 50% vs DLIR-H, and P_3 compares DLIR-M vs DLIR-H. *P* values were calculated using the Friedman test with Bonferroni-Dunn post-hoc analysis.

ASIR-V = adaptive statistical iterative reconstruction-V, DLIR-H = high-strength deep learning image reconstruction, DLIR-M = medium-strength deep learning image reconstruction.

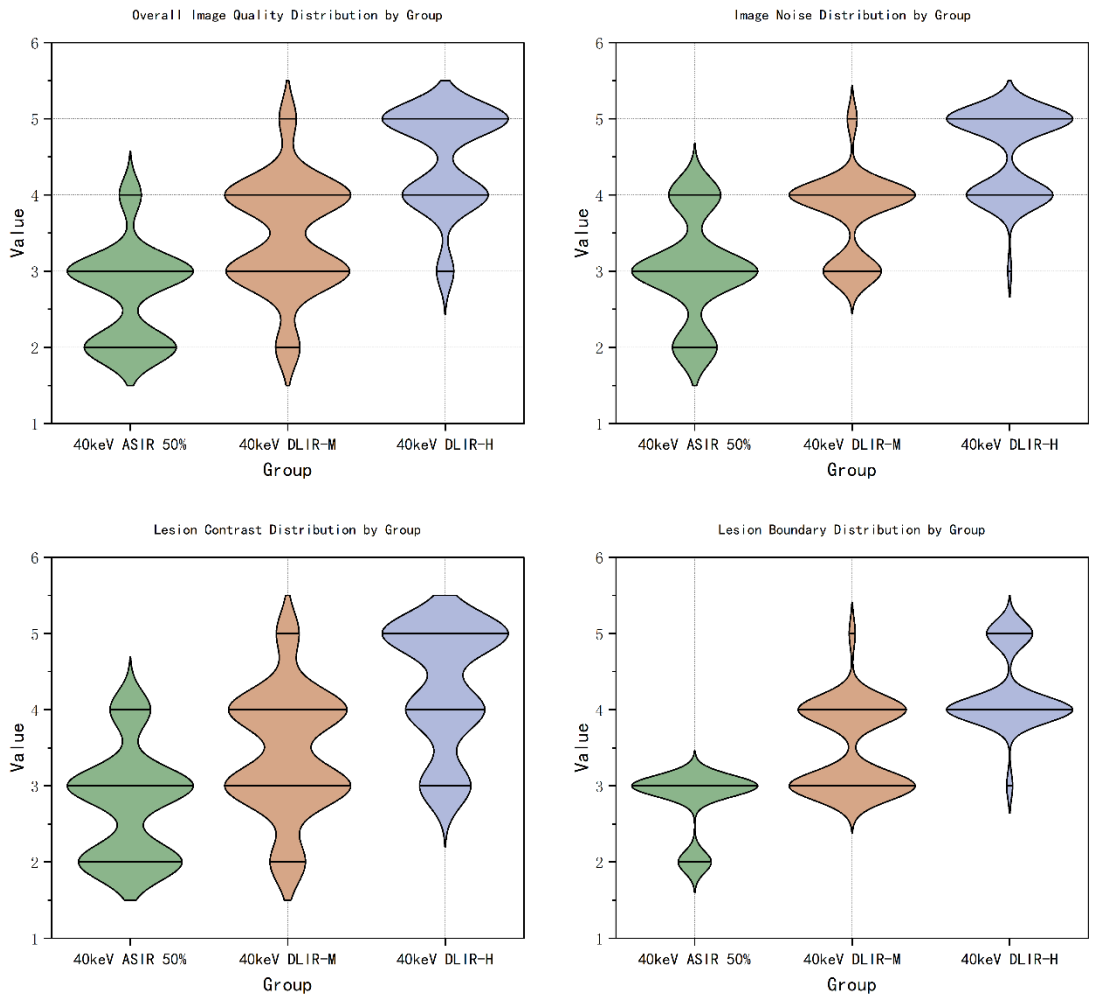


Figure 3: Qualitative subjective image quality assessment using a 5-point Likert scale across reconstruction groups.

Violin plots show the distribution of subjective scores for **(a)** overall image quality, **(b)** image noise, **(c)** lesion contrast, and **(d)** lesion boundary for the 40-keV virtual monoenergetic images. Assessment was performed independently by two senior radiologists. Within each plot, solid horizontal lines indicate the median scores, and dashed lines represent the interquartile ranges. The DLIR-H group yielded significantly higher scores in all categories compared with the DLIR-M and ASIR-V 50% groups (all $P < .001$). Note that DLIR-H scores were predominantly clustered at 5 (excellent), while ASIR-V 50% scores centered around 3 (acceptable for clinical diagnosis), demonstrating the superior performance of high-strength deep learning reconstruction in suppressing noise while maintaining lesion conspicuity.

ASIR-V = adaptive statistical iterative reconstruction-V, DLIR-H = high-strength deep learning image reconstruction, DLIR-M = medium-strength deep learning image reconstruction.

Analysis of Subjective Score Distribution

The distribution of subjective quality ratings is illustrated in **Figure 4**. For all four categories (overall image quality, image noise, lesion contrast, and lesion boundary), the proportion of high-quality ratings (score ≥ 4) increased progressively from ASIR-V 50% to DLIR-H. Specifically, DLIR-H yielded scores ≥ 4 for nearly all patients across all categories, with no cases receiving a score below 3. In contrast, the ASIR-V 50% group demonstrated a substantial proportion of suboptimal ratings (score < 3), particularly in overall image quality and lesion contrast (approximately 40% of ratings). Notably, for lesion boundary definition, ASIR-V 50% failed to achieve a score ≥ 4 in any patient, whereas DLIR-H achieved scores ≥ 4 in the vast majority of cases.

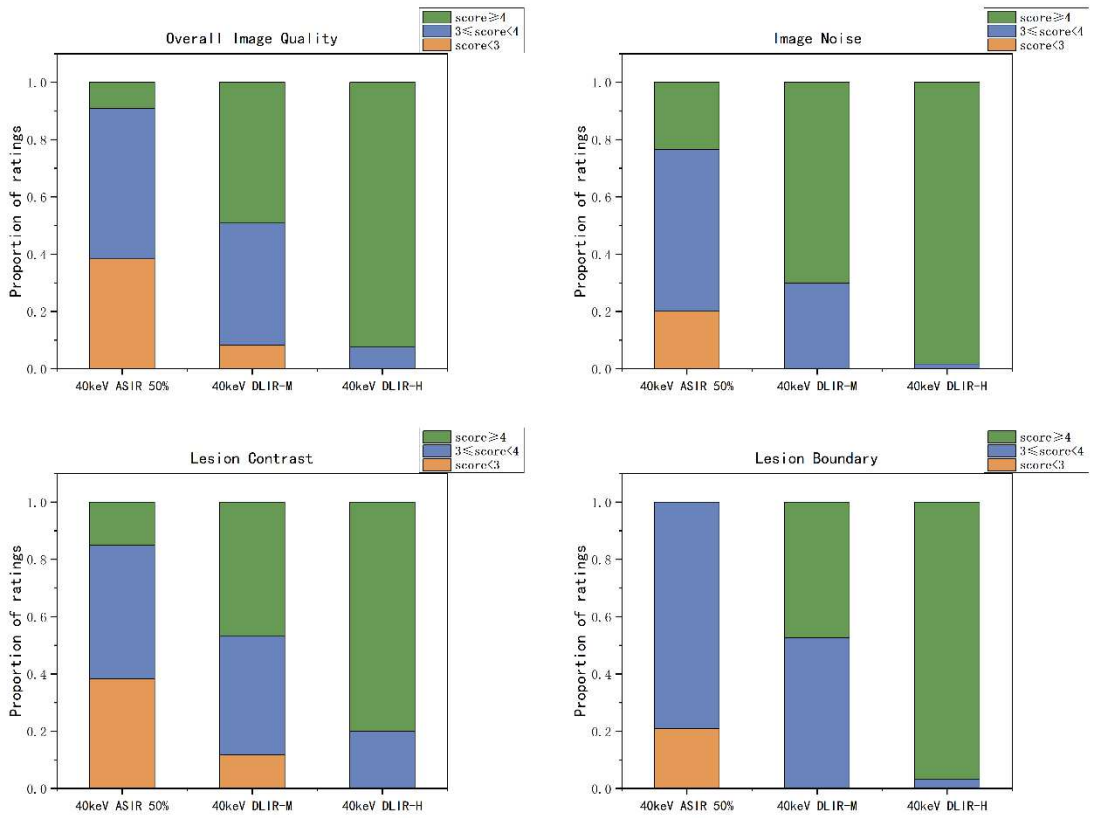


Figure 4: Stacked bar charts illustrating the proportion of subjective image quality ratings.

The distribution of scores for **(a)** overall image quality, **(b)** image noise, **(c)** lesion contrast, and **(d)** lesion boundary is compared across ASIR-V 50%, DLIR-M, and DLIR-H reconstruction groups at 40 keV. Ratings are categorized as ≥ 4 (green, indicating good or excellent quality), 3 to < 4 (blue, indicating acceptable quality), and < 3 (orange, indicating suboptimal quality). Note that DLIR-H consistently achieves the highest proportion of "good or excellent" ratings across all parameters. Conversely, ASIR-V 50% shows the highest frequency of suboptimal scores (< 3), particularly for lesion contrast and overall image quality, highlighting the limitations of iterative reconstruction in managing 40-keV noise.

ASIR-V = adaptive statistical iterative reconstruction-V, DLIR-H = high-strength deep learning image reconstruction, DLIR-M = medium-strength deep learning image reconstruction.

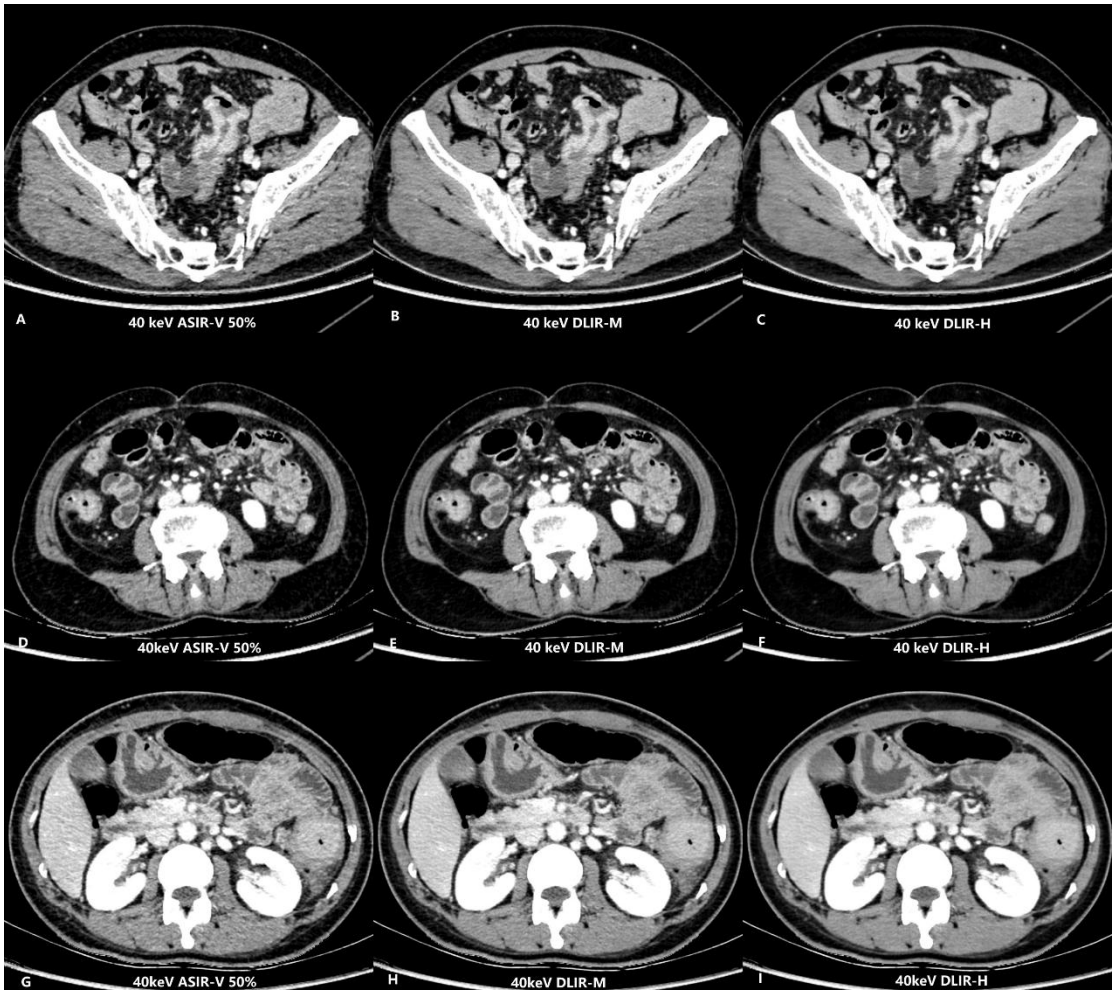


Figure 5: Representative axial 40-keV virtual monoenergetic images (VMI) of colon cancer reconstructed with different algorithms.

(A–C) Axial images of a 71-year-old man (BMI, 25.7 kg/m^2) with sigmoid colon adenocarcinoma (cT3NxMx). Image noise is markedly reduced, and the tumor-to-fat interface is more clearly defined in the **(C)** DLIR-H reconstruction compared with the **(A)** ASIR-V50% and **(B)** DLIR-M images. Quantitative analysis for this patient showed a standard deviation (SD) of 32.0, 26.6, and 20.1 HU; a SNR of 5.79, 7.91, and 11.87; and a CNR of 3.21, 4.34, and 6.46 for **A**, **B**, and **C**, respectively.

(D–F) Axial images of a 63-year-old woman (BMI, 21.6 kg/m^2) with ascending colon adenocarcinoma. Note the improved visualization of the thickened bowel wall and the surrounding mesenteric vessels in the **(F)** DLIR-H image. Corresponding SD values were 46.9, 37.8, and 30.5 HU; SNR values were 6.54, 7.98, and 11.40; and CNR values were 1.61, 1.96, and 2.78 for **D**, **E**, and **F**, respectively.

(G–I) Axial images of a 45-year-old woman (BMI, 21.7 kg/m^2) with descending colon cancer and regional lymphadenopathy. High-strength DLIR **(I)** provides superior conspicuity of the small peritumoral lymph nodes and fine vascular branches, which are partially obscured by noise in the **(G)** ASIR-V50% reconstruction. Corresponding SD values were 36.5, 28.4, and 20.2 HU; SNR values were 6.08, 7.76, and 11.02; and CNR values were 3.09, 4.00, and 5.70 for **G**, **H**, and **I**, respectively.

ASIR-V = adaptive statistical iterative reconstruction-V, DLIR-H = high-strength deep learning image reconstruction, DLIR-M = medium-strength deep learning image reconstruction, HU = Hounsfield unit.

Discussion

In this study, we found that 40-keV VMI reconstructed with DLIR-H provided superior objective and subjective image quality for primary tumors, feeding arteries, and regional lymph nodes compared with standard-of-care ASIR-V. Although DLIR-H resulted in a slight reduction in the objective ERS—indicating a minor trade-off in edge steepness—it significantly improved diagnostic confidence by mitigating the severe photon starvation and image noise characteristic of 40-keV VMI.

The clinical implementation of low-energy VMI, particularly at 40 keV, is driven by the necessity to maximize iodine attenuation in colorectal imaging. At 40 keV, the mean photon energy approximates the iodine K-edge (33.2 keV), resulting in a substantial increase in the CNR. This physiological boost facilitates the identification of subtle morphological features, such as extramural venous invasion (EMVI) and early serosal penetration[8, 20]. However, hybrid IR, such as ASIR-V, often fails to adequately manage the severe photon starvation at this energy level, frequently resulting in a 'grainy' or 'blotchy' texture that obscures the critical tumor-to-fat interface[11, 12]. In our study, DLIR-H achieved a nearly 82% reduction in image noise compared with ASIR-V, which is consistent with recent findings in low-dose abdominal CT where DLIR outperformed hybrid IR by more effectively differentiating anatomical signals

from noise through deep convolutional neural networks[16].

A salient finding in our quantitative analysis was the discrepancy between objective edge steepness and subjective boundary definition. Although the ERS—a surrogate for mathematical edge steepness—was higher in the ASIR-V group, radiologists assigned the highest subjective scores for 'lesion boundary' to the DLIR-H reconstructions. This phenomenon, often termed the 'sharpness-clarity paradox', is frequently observed in the evaluation of advanced reconstruction algorithms[12]. While hybrid IR (ASIR-V) maintains the mathematical steepness of the edge transition, the accompanying high-frequency noise tends to obscure or 'clutter' the anatomical interface. Conversely, DLIR-H effectively suppresses these noise components; although this results in a slightly smoother transition profile (lower ERS), it ultimately enhances the conspicuity of the margin by optimizing the local contrast between the tumor and the surrounding pericolic fat[21]. This distinction is clinically relevant for the substaging of T3 colorectal lesions, where the perceived clarity of the serosal margin is of greater diagnostic value than the mathematical steepness of the edge rise.

The multi-target assessment strategy adopted in our study—encompassing the primary tumor, mesenteric vasculature, and regional nodes—offers a comprehensive evaluation of the diagnostic utility of DLIR in colorectal oncology. High-fidelity visualization of the feeding arteries, such as the ileocolic or right colic artery, is paramount for preoperative surgical mapping and the identification of anatomical variants prior to D3 lymphadenectomy[22]. Furthermore, the substantial increase in SNR for regional lymph nodes achieved with DLIR-H suggests potential for improved sensitivity in detecting occult nodal metastases, which is a critical determinant of N-staging accuracy. Importantly, the synergy between 40-keV VMI and DLIR-H facilitated high-quality assessment even with a reduced iodine protocol (1.0 mL/kg). This renal-protective approach is of significant clinical value for patients with impaired kidney function or those requiring longitudinal surveillance, effectively balancing diagnostic confidence with patient safety[23].

Limitations

Our study had several limitations. First, the retrospective, single-center design and moderate sample size ($N = 60$) may limit the generalizability of our findings to other CT platforms or institutional protocols. Second, while we demonstrated substantial improvements in objective and subjective image quality, we did not directly evaluate the diagnostic performance—specifically the sensitivity and specificity for T-substaging and extramural venous invasion (EMVI)—against a pathological reference standard. Future prospective studies are required to determine if these quality improvements translate into higher staging accuracy. Third, our assessment was primarily focused on the portal venous phase; the utility of DLIR in other phases (e.g., the arterial phase) for vascular assessment warrants further exploration.

Conclusion

In conclusion, DLIR-H significantly improves the image quality of 40-keV virtual monoenergetic CT in colon cancer compared with adaptive statistical iterative reconstruction. By providing an optimal balance between robust noise suppression and anatomical edge preservation, DLIR-H enhances the delineation of the primary tumor, regional lymph nodes, and the mesenteric vasculature. This combination facilitates the clinical transition toward low-energy, low-iodine spectral CT protocols in colorectal oncology, potentially improving patient safety without compromising diagnostic confidence.

References

1. Bray, F., et al., *Global cancer statistics 2022: GLOBOCAN estimates of incidence and mortality worldwide for 36 cancers in 185 countries.* CA Cancer J Clin, 2024. **74**(3): p. 229–263.
2. Siegel, R.L., et al., *Colorectal cancer statistics, 2023.* CA Cancer J Clin, 2023. **73**(3): p. 233–254.
3. Cervantes, A., et al., *Metastatic colorectal cancer: ESMO Clinical Practice*

Guideline for diagnosis, treatment and follow-up. Ann Oncol, 2023. **34**(1): p. 10–32.
4. Nougaret, S., et al., *MRI of the Rectum: A Decade into DISTANCE, Moving to DISTANCED.* Radiology, 2025. **314**(1): p. e232838.
5. Zhu, L., et al., *Optimization and Initial Diagnostic Performance of Photon-Counting Detector CT for Rectal Cancer T Staging.* Radiology, 2025. **317**(2): p. e250231.
6. Chang, K.J., et al., *Radiologic T staging of colon cancer: renewed interest for clinical practice.* Abdom Radiol (NY), 2023. **48**(9): p. 2874–2887.
7. Chen, F.X., et al., *Diagnostic accuracy of dual-layer spectral computed tomography virtual monoenergetic imaging with multiplanar reformation for T-staging of colorectal cancer.* World J Gastroenterol, 2025. **31**(32): p. 110573.
8. Arico, F.M., et al., *Virtual monoenergetic dual-layer dual-energy CT images in colorectal cancer: CT diagnosis could be improved?* Radiol Med, 2023. **128**(8): p. 891–899.
9. Nagayama, Y., et al., *Dual-layer dual-energy computed tomography for the assessment of hypovascular hepatic metastases: impact of closing k-edge on image quality and lesion detectability.* Eur Radiol, 2019. **29**(6): p. 2837–2847.
10. Franco, P.N., et al., *Principles and Applications of Dual-Layer Spectral CT in Gastrointestinal Imaging.* Diagnostics (Basel), 2023. **13**(10).
11. Chung, R., et al., *Dual-Energy Computed Tomography: Technological Considerations.* Radiol Clin North Am, 2023. **61**(6): p. 945–961.
12. Koetzier, L.R., et al., *Deep Learning Image Reconstruction for CT: Technical Principles and Clinical Prospects.* Radiology, 2023. **306**(3): p. e221257.
13. Huang, X., et al., *Improving image quality with deep learning image reconstruction in double-low-dose head CT angiography compared with standard dose and adaptive statistical iterative reconstruction.* Br J Radiol, 2023. **96**(1143): p. 20220625.
14. ; Available from: https://www.gehealthcare.com/-/jssmedia/gehc/us/images/products/computed-tomography/truefidelity/related-content/new/truefidelity-for-gsi-whitepaper-digital-jb19879xx-final.pdf?rev=-1.
15. Pauthe, A., et al., *Impact of deep learning reconstructions on image quality and liver lesion detectability in dual-energy CT: An anthropomorphic phantom study.* Med Phys, 2025. **52**(4): p. 2257–2268.
16. Cao, J., et al., *Multi-reader multiparametric DECT study evaluating different strengths of iterative and deep learning-based image reconstruction techniques.* Eur Radiol, 2025. **35**(2): p. 885–896.
17. Ryu, J.K., et al., *Improved stent sharpness evaluation with super-resolution deep learning reconstruction in coronary CT angiography.* Br J Radiol, 2024. **97**(1159): p. 1286–1294.
18. Wang, S.F., et al., *Image Quality Optimization in 60 kVp Head-Neck CTA: A Comparative Study of FBP, ClearView, and ClearInfinity Reconstruction Algorithms.* Curr Med Sci, 2025. **45**(6): p. 1504–1512.

19. Zhang, H., et al., *Image quality improvement in head and neck angiography based on dual-energy CT and deep learning.* BMC Med Imaging, 2025. **25**(1): p. 115.
20. Jia, Z., et al., *Performance of dual-layer spectrum CT virtual monoenergetic images to assess early rectal adenocarcinoma T-stage: comparison with MR.* Insights Imaging, 2024. **15**(1): p. 11.
21. Cao, L., et al., *Improving spatial resolution and diagnostic confidence with thinner slice and deep learning image reconstruction in contrast-enhanced abdominal CT.* Eur Radiol, 2023. **33**(3): p. 1603–1611.
22. Zhong, J., et al., *Deep learning image reconstruction for low-kiloelectron volt virtual monoenergetic images in abdominal dual-energy CT: medium strength provides higher lesion conspicuity.* Acta Radiol, 2024. **65**(9): p. 1133–1146.
23. Yoshida, K., et al., *Low tube voltage and deep-learning reconstruction for reducing radiation and contrast medium doses in thin-slice abdominal CT: a prospective clinical trial.* Eur Radiol, 2024. **34**(11): p. 7386–7396.

Supplementary Files

This is a list of supplementary files associated with this preprint. Click to download.

- SupplementaryTableE1.QualitativeSubjectiveImageQualityScale2.xlsx